International Journal of Fracture **112:** 23–41, 2001.

The boundary-layer effect on the crack tip field in mechanism-based strain gradient plasticity

M. SHI[1], Y. HUANG[1,*], H. JIANG[2], K. C. HWANG[2] and MING LI[3]
[1]*Department of Mechanical and Industrial Engineering, University of Illinois, Urbana, IL 61801, U.S.A.*
[2]*Failure Mechanics Laboratory, Department of Engineering Mechanics, Tsinghua University, Beijing 100084, China*
[3]*Alcoa Technical Center, Alcoa Center, PA 15069, U.S.A.*

Received 27 February 2001; accepted in revised form 29 May 2001

Abstract. The theory of mechanism-based strain gradient (MSG) plasticity involves two material length parameters, namely the intrinsic material length l and the mesoscale cell size l_ε, which are on the order of a few microns and 0.1 μm, respectively. Prior studies suggest that l_ε has essentially no effect on the macroscopic quantities, but it may affect the local stress distribution. We demonstrate in this paper that there is a boundary layer effect associated with l_ε in MSG plasticity, and the thickness of the boundary layer is on the order of l_ε^2/l. By neglecting this boundary layer effect, a stress-dominated asymptotic field around a crack tip in MSG plasticity is obtained. This asymptotic field is valid at a distance to the crack tip between l_ε and l (i.e., from 0.1 μm to a few microns). The stress in this asymptotic field has an approximate singularity of $r^{-2/3}$, which is more singular than not only the HRR field in classical plasticity but also the classical elastic K field ($r^{-1/2}$). The stress level in this asymptotic field is two to three times higher than the HRR field, which provides an alternative mechanism for cleavage fracture in ductile materials observed in experiments.

Key words: Boundary layer, crack tip singularity, strain gradient plasticity, Taylor model.

1. Introduction

Metallic materials display significant size effect at the micron and sub-micron scales, as observed in the experiments of micro-twist (Flect et al., 1994), micro-bend (Stolken and Evans, 1998) and micro-indentation (Nix, 1989, 1997; de Guzman et al., 1993; Stelmashenko et al., 1993; Ma and Clarke, 1995; Poole et al., 1996; McElhaney et al., 1998; Suresh et al., 1999). Direct dislocation simulations also show strong size effect of metallic materials under various loading conditions at the micron scale (Cleveringa et al., 1997, 1998, 1999a, b, 2000; Needleman, 2000). The classical theory of plasticity cannot explain the observed size effect since its constitutive law contains no intrinsic material length. This has motivated the development of strain gradient plasticity theories (Fleck and Hutchinson, 1993; Fleck et al., 1994; Gao et al., 1999b; Shu and Fleck, 1999; Acharya and Bassani, 2000; Acharya and Beaudoin, 2000; Chen and Wang, 2000; Huang et al., 2000a, b; Dai and Parks, 2001) based on the concept of geometrically necessary dislocations in dislocation mechanics (e.g., Nye, 1953; Cottrell, 1964; Ashby, 1970; Arsenlis and Parks, 1999; Gurtin, 2000). The theories of strain gradient plasticity have already shown some success to model the size dependence of material behavior at the micron-scale. For example, Begley and Hutchinson (1998) and Huang et al. (2000b) showed respectively that the phenomenological theory of strain gradient plasticity (Fleck and

*Author for correspondence. E-mail: huang9@uiuc.edu

Hutchinson, 1997) and the mechanism-based strain gradient (MSG) plasticity theory derived from the Taylor dislocation model (1938) agree well with McElhaney et al.'s (1998) micro-indentation hardness experiments. Gao et al. (1999a) also showed that MSG plasticity theory agrees well with the micro-twist (Fleck et al., 1994) and micro-bend experiments (Stolken and Evans, 1998). There are also earlier works on strain gradient plasticity that were proposed in order to avoid a spurious solution for the localized zone and an excessive mesh dependence in classical plasticity (e.g., Aifantis, 1984; Lasry and Belytschko, 1988; Zbib and Aifantis, 1988; Mühlhaus and Aifantis, 1991; de Borst and Mühlhaus, 1991, 1992; Aifantis, 1992; Sluys et al., 1993).

The theories of strain gradient plasticity may also be important to another class of microscale phenomena, namely, the cleavage fracture in ductile materials. In a remarkable series of experiments, Elssner et al. (1994) measured both the macroscopic fracture toughness and atomic work of separation of an interface between a single crystal niobium and a single crystal sapphire. They found the macroscopic fracture toughness to be two to three orders of magnitude higher than the atomic work of separation, indicating significant plastic deformation in niobium. According to models based on classical plasticity, the maximum stress level that can be achieved around a crack tip in metals is no more than 4–5 times the initial yield stress σ_Y (Hutchinson, 1997). However, Elssner et al. (1994) observed that the crack tip remained atomistically sharp, i.e., no crack tip blunting even though there was significant plastic deformation in niobium. Cleavage fracture in presence of significant plastic flow has also been observed in other material systems (e.g., Oh et al., 1987; Wang and Anderson, 1991; Beltz and Wang, 1992; Korn et al., 1992; O'Dowd et al., 1992; Bagchi et al., 1994; Bagchi and Evans, 1996). The stress level for atomic decohesion of a lattice or a strong interface is typically the theoretical shear strength, which is around 10% of the elastic shear modulus, or approximately 10 times the initial yield stress σ_Y. Classical plasticity theory (4–5 σ_Y) clearly falls short to reach this stress level (10 σ_Y) triggering atomic decohesion. This motivated Suo et al. (1993), Beltz et al. (1996) and Wei and Hutchinson (1999) to develop an elastic strip model, i.e., the crack tip was surrounded by a dislocation-free elastic strip with the strip height on the order of average dislocation spacing. The stress level around the elastic crack tip increased significantly since the elastic square-root singularity was much higher (i.e., more singular) than that around a crack tip in plasticity.

The theories of strain gradient plasticity may provide an alternative approach to bridge the gap between plasticity models and cleavage fracture experiments in ductile materials. Using Fleck and Hutchinson's (1997) phenomenological theory of strain gradient plasticity, Wei and Hutchinson (1997) and Chen et al. (1999) found respectively that the stress level around a quasi-statically propagating crack tip and around a stationary crack tip increased significantly due to the strain gradient effect, though the asymptotic crack tip field may not have the domain of physical validity (Chen et al., 1999). Shi et al. (2000) used MSG plasticity theory (Gao et al., 1999b; Huang et al., 2000a, b) to investigate the asymptotic crack tip field and found that, *within a distance of* 0.1 μm *to the crack tip, the asymptotic field in MSG plasticity is not separable*, i.e.,

$$\sigma_{ij} \neq \frac{A}{r^{\lambda}} \widetilde{\sigma}_{ij}(\theta) \quad \text{for} \quad r < 0.1\ \mu\text{m}, \tag{1}$$

where (r, θ) are the polar coordinates centered at the crack tip, σ_{ij} is the stress and $\widetilde{\sigma}_{ij}(\theta)$ the corresponding angular function, λ the power of stress singularity, and A the amplitude factor depending on the applied loading, specimen geometry and material properties. Jiang

et al. (2001) used the finite element method to investigate the crack tip field in MSG plasticity, with the classical elastic K field being imposed as the remote boundary condition in the numerical analysis. Moving away from the remote boundary towards the crack tip, the transition was observed from the classical elastic K field through the HRR field (Hutchinson, 1968; Rice and Rosengren, 1968) in classical plasticity to a new crack tip field in MSG plasticity. *At a distance larger than* 0.1 μm *to the crack tip, the stress level is significantly higher* (2–3 *times*) *than its counterpart in the HRR field*. This significant stress increase due to the strain gradient effect provides an alternative mechanism for cleavage fracture in ductile materials. Contrary to Shi et al.'s (2000) asymptotic analysis which holds for a distance to the crack tip $r < 0.1$ μm, the numerical results of Jiang et al. (2001) showed that the stress field seems to be separable at a distance $r > 0.1$ μm to the crack tip. Moreover, the crack tip stress singularity λ in (1) is larger than $\frac{1}{2}$, i.e., the stress field in MSG plasticity is more singular than the classical elastic K field.

It is puzzling why the crack tip field in MSG plasticity is not separable within a distance of 0.1 μm to the crack tip (Shi et al., 2000), but becomes separable at a distance larger than 0.1 μm and is more singular than the square-root singularity. As shown in the present paper, the above puzzle is due to the boundary layer effect in MSG plasticity. We first summarize the theory of MSG plasticity in Section 2, followed by an example to demonstrate the boundary layer effect in Section 3. The crack tip field in MSG plasticity is then studied in Section 4.

2. Mechanism-based strain gradient plasticity theory

The theory of mechanism-based strain gradient (MSG) plasticity (Gao et al., 1999b; Huang et al., 2000a) is summarized in this section. It has incorporated the modifications proposed by Huang et al. (2000b) based on polycrystalline plasticity.

2.1. Generalized strains and stresses

In a Cartesian reference frame x_i, the strain tensor ε_{ij} and strain gradient tensor η_{ijk} are related to the displacement u_i by

$$\varepsilon_{ij} = \tfrac{1}{2}\left(u_{i,j} + u_{j,i}\right), \quad \eta_{ijk} = u_{k,ij}, \tag{2}$$

which have the symmetry $\varepsilon_{ij} = \varepsilon_{ji}$ and $\eta_{ijk} = \eta_{jik}$. Since the elastic deformation is negligible around the crack tip, the incompressibility requries $\varepsilon_{ii} = 0$ and $\eta_{kii} = 0$. The work increment per unit volume of an incompressible solid is $\delta w = \sigma'_{ij}\delta\varepsilon_{ij} + \tau'_{ijk}\delta\eta_{ijk}$, where the symmetric deviatoric Cauchy stress σ'_{ij} is the work conjugate of the variation of strain $\delta\varepsilon_{ij}$, and $\sigma'_{ii} = 0$; the symmetric deviatoric higher-order stress τ'_{ijk} is the work conjugate of the variation of strain gradient $\delta\eta_{ijk}$, and $\tau'_{kii} = 0$.

2.2. Equilibrium equations and boundary conditions

The equilibrium equations for an incompressible solid can be written as (Fleck and Hutchinson, 1997)

$$\sigma'_{ik,i} - \tau'_{ijk,ij} + H_{,k} + f_k = 0, \tag{3}$$

where f_k is the body force and H is the combined measure of the hydrostatic stress and hydrostatic higher-order stress. The stress traction and higher-order stress traction on the surface of the body are

$$\begin{aligned}\hat{t}_k = \; & Hn_k + n_i\left(\sigma'_{ik} - \tau'_{ijk,j}\right) + D_k\left(n_i n_j n_p \tau'_{ijp}\right) \\ & -D_j\left(n_i \tau'_{ijk}\right) + \left(n_i n_j \tau'_{ijk} - n_k n_i n_j n_p \tau'_{ijp}\right)\left(D_q n_q\right),\end{aligned} \tag{4}$$

$$\hat{r}_k = n_i n_j \tau'_{ijk} - n_k n_i n_j n_p \tau'_{ijp}, \tag{5}$$

where n_i is the unit normal to the surface and D_j is the surface-gradient operator given by $D_j = \left(\delta_{jk} - n_j n_k\right)(\partial/\partial x_k)$. For the special case where the surface has edges, there is a line traction that must be taken into account (Fleck and Hutchinson, 1997). Suppose the surface has an edge C, formed by the intersection of two smooth surface segments $S^{(1)}$ and $S^{(2)}$. The unit normal to segment $S^{(i)}$ $(i = 1, 2)$ is designated $n^{(i)}$, while the unit tangent $c^{(i)}$ along the edge C is defined with segment $S^{(i)}$ to the left. The line traction is

$$\hat{p}_k = \sum\left(n_i k_j \tau'_{ijk} - k_k n_i n_j n_p \tau'_{ijp}\right), \tag{6}$$

where the summation is over both surfaces $S^{(1)}$ and $S^{(2)}$ at the edge C, and $k^{(i)}$ $(i = 1, 2)$ is the unit outward normal to C lying within the surface $S^{(i)}$ given by $k^{(i)} = c^{(i)} \times n^{(i)}$ $(i = 1, 2)$.

2.3. Constitutive equations

The uniaxial stress-strain relation can be written as

$$\sigma = \sigma_{\text{ref}} f(\varepsilon), \tag{7}$$

where σ_{ref} is a reference stress in uniaxial tension. For most ductile materials, the function f can be written as a power law relation $f(\varepsilon) = \varepsilon^N$, where N is the plastic work hardening exponent $(0 \leq N < 1)$. The flow stress, after incorporating the strain gradient effects, is obtained from Taylor's dislocation model (Taylor, 1938) as (Nix and Gao, 1998; Huang et al., 2000b)

$$\sigma = \sigma_{\text{ref}}\sqrt{f^2(\varepsilon) + l\eta}, \tag{8}$$

where $l\eta$ and $f^2(\varepsilon)$ represent the contributions from geometrically necessary and statistically stored dislocations, respectively, $\varepsilon = \sqrt{\frac{2}{3}\,\varepsilon_{ij}\,\varepsilon_{ij}}$ is the effective strain and $\eta = \frac{1}{2}\sqrt{\eta_{ijk}\,\eta_{ijk}}$ is the effective strain gradient, l is the intrinsic material length in strain gradient plasticity given in terms of shear modulus μ and Burgers vector b by

$$l = 18\alpha^2\left(\frac{\mu}{\sigma_{\text{ref}}}\right)^2 b, \tag{9}$$

and α is an empirical material constant in Taylor's dislocation model (1938) ranging between 0.1 and 0.5. For typical metallic materials, the intrinsic material length l is on the order of a few microns.

The constitutive equations for the deformation theory of MSG plasticity are

$$\sigma'_{ij} = \frac{2\varepsilon_{ij}}{3\varepsilon}\sigma, \tag{10}$$

$$\tau'_{ijk} = l_\varepsilon^2\left[\frac{\sigma}{\varepsilon}(\Lambda_{ijk} - \Pi_{ijk}) + \frac{\sigma_{\text{ref}}^2 f(\varepsilon) f'(\varepsilon)}{\sigma}\Pi_{ijk}\right], \tag{11}$$

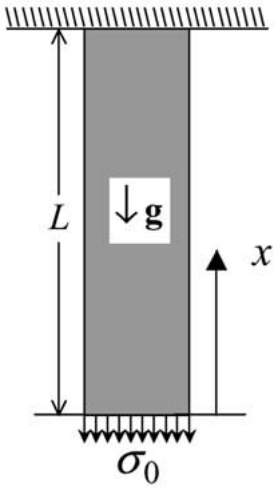

Figure 1. A schematic diagram of a bar subjected to a constant body force g and applied stress σ_0 at the free end.

where the flow stress σ is given in (8), Λ_{ijk} and Π_{ijk} are given by

$$\Lambda_{ijk} = \tfrac{1}{72}[2\eta_{ijk} + \eta_{kij} + \eta_{kji} - \tfrac{1}{4}(\delta_{ik}\eta_{ppj} + \delta_{jk}\eta_{ppi})], \tag{12}$$

$$\Pi_{ijk} = \frac{1}{54}\frac{\varepsilon_{mn}}{\varepsilon^2}\left[\varepsilon_{ik}\eta_{jmn} + \varepsilon_{jk}\eta_{imn} - \tfrac{1}{4}(\delta_{ik}\varepsilon_{jp} + \delta_{jk}\varepsilon_{ip})\eta_{pmn}\right], \tag{13}$$

l_ε is the mesoscale cell size introduced in MSG plasticity and is on the order of average dislocation spacing at initial plastic yielding, i.e.,

$$l_\varepsilon \sim \frac{\mu}{\sigma_Y} b, \tag{14}$$

and σ_Y is the initial yield stress in uniaxial tension. For typical metallic materials, l_ε is less than 0.1 μm and is therefore significantly less than the intrinsic material length l in (9).

It can be verified that the parameter l_ε^2 scales the highest order derivative in the equilibrium equation (3) after the constitutive law (10) and (11) are substituted into (3). Since l_ε is much smaller than the intrinsic material length l, MSG plasticity may have a boundary-layer type solution. As shown in the next section, the boundary layer thickness is on the order of l_ε^2/l, which is less than 10 nm for typical metallic materials. This is, in fact, consistent with the conclusion established in prior studies (Huang et al., 2000a, b) that the parameter l_ε does not affect the macroscopic quantities (e.g., bending moment, torque, indentation hardness, applied stress), but it may significantly change the local stress field near the boundary. In the following section, we use a simple and analytic example to demonstrate such a boundary layer effect in MSG plasticity.

3. An example of a boundary layer in MSG Plasticity

We consider a simple bar subjected to a constant body force g and a uniform stress σ_0 at the free end along the direction of the bar (Figure 1). For simplicity, we assume the material is incompressible such that the non-zero components of the strain tensor are

$$\varepsilon_{11} = -2\varepsilon_{22} = -2\varepsilon_{33} = \varepsilon(x), \tag{15}$$

where ε is the effective strain and the coordinate x $(= x_1)$ is along the direction of the bar. The non-vanishing components of the strain gradient tensor and the effective strain gradient η are obtained from (2),

$$\begin{aligned} \eta_{111} &= 2\eta_{221} = 2\eta_{331} = -2\eta_{122} = -2\eta_{212} = -2\eta_{133} = -2\eta_{313} = \frac{\mathrm{d}\varepsilon}{\mathrm{d}x}, \\ \eta &= \sqrt{\frac{5}{8}}\frac{\mathrm{d}\varepsilon}{\mathrm{d}x}. \end{aligned} \tag{16}$$

The constitutive law (10) and (11) give the non-vanishing components of the deviatoric stress and deviatoric higher-order stress tensor as

$$-\tfrac{1}{2}\sigma'_{11} = \sigma'_{22} = \sigma'_{33} = -\tfrac{1}{3}\sigma, \tag{17}$$

$$-\tfrac{1}{2}\tau'_{111} = \tau'_{122} = \tau'_{212} = \tau'_{133} = \tau'_{313} = -\frac{l_\varepsilon^2}{48}\frac{\mathrm{d}\varepsilon}{\mathrm{d}x}\frac{\sigma_{\mathrm{ref}}^2 f(\varepsilon) f'(\varepsilon)}{\sigma}, \tag{18}$$

where the flow stress σ is obtained from (8)

$$\sigma = \sigma_{\mathrm{ref}}\sqrt{f^2(\varepsilon) + \sqrt{\frac{5}{8}} l \frac{\mathrm{d}\varepsilon}{\mathrm{d}x}}. \tag{19}$$

The hydrostatic stress H can be determined from the traction-free boundary condition on the lateral surface as

$$H = -\sigma'_{22} + 2\frac{\mathrm{d}\tau'_{122}}{\mathrm{d}x}. \tag{20}$$

The substitution of the above constitutive relations into the equilibrium Equation (3) yields the following ordinary differential equation (*ODE*) for the strain $\varepsilon(x)$,

$$\frac{\mathrm{d}\sigma}{\mathrm{d}x} - \frac{l_\varepsilon^2}{12}\frac{\mathrm{d}^2}{\mathrm{d}x^2}\left[\frac{\mathrm{d}\varepsilon}{\mathrm{d}x}\frac{\sigma_{\mathrm{ref}}^2 f(\varepsilon) f'(\varepsilon)}{\sigma}\right] = g. \tag{21}$$

The stress traction at the free end ($x = 0$) is

$$\widehat{t}_1\big|_{x=0} = \left(H + \sigma'_{11} - \frac{\mathrm{d}\tau'_{111}}{\mathrm{d}x}\right)\bigg|_{x=0} = \left(\sigma - 2\frac{\mathrm{d}\tau'_{111}}{\mathrm{d}x}\right)\bigg|_{x=0} = \sigma_0. \tag{22}$$

At the fixed end, the axial displacement should vanish,

$$u|_{x=L} = 0, \tag{23}$$

where L is the length of the bar. The higher-order boundary conditions are the vanishing of higher-order stress tractions and line tractions at both ends, which give

$$l_\varepsilon^2 \frac{\mathrm{d}\varepsilon}{\mathrm{d}x}\bigg|_{x=0} = 0, \tag{24}$$

and

$$l_\varepsilon^2 \frac{\mathrm{d}\varepsilon}{\mathrm{d}x}\bigg|_{x=L} = 0. \tag{25}$$

Without losing generality, we take the plastic work hardening exponent $N = \frac{1}{2}$ $\left[f(\varepsilon) = \varepsilon^{1/2}\right]$ in order to find an analytical solution in this section that clearly shows the structure of a boundary layer in MSG plasticity. The governing Equation (21), after integrating with respect to x and using the stress traction boundary condition (22), yields

$$\frac{\sigma}{\sigma_{\text{ref}}} - \frac{l_\varepsilon^2}{24}\frac{\mathrm{d}}{\mathrm{d}x}\left[\frac{\mathrm{d}\varepsilon}{\mathrm{d}x}\left(\frac{\sigma}{\sigma_{\text{ref}}}\right)^{-1}\right] = \frac{gx + \sigma_0}{\sigma_{\text{ref}}}, \tag{26}$$

where

$$\frac{\sigma}{\sigma_{\text{ref}}} = \left(\varepsilon + \sqrt{\frac{5}{8}}l\frac{\mathrm{d}\varepsilon}{\mathrm{d}x}\right)^{1/2}. \tag{27}$$

Equation (26) constitutes a second-order ODE for the effective strain ε with two higher-order boundary conditions in (24) and (25). Once ε is determined, its integration plus the displacement boundary condition (23) at the fixed end gives the displacement in the bar. By neglecting the strain gradient and higher-order stress, we obtain the strain distribution for the classical plasticity theory

$$\varepsilon_{\text{classical}} = \left(\frac{gx + \sigma_0}{\sigma_{\text{ref}}}\right)^2. \tag{28}$$

It is recalled that the parameter l_ε scaling the highest order derivatives in (26) is much less than the intrinsic material length l in MSG plasticity, i.e., $l_\varepsilon \ll l$. Accordingly, the solution for MSG plasticity may have boundary layers near the ends ($x = 0, L$) with the layer thickness on the order of l_ε^2/l. It becomes clear later that the boundary layer is near the fixed end ($x = L$). Away from the boundary layer ($x < L$), the l_ε^2 terms are negligible and (26) becomes

$$\varepsilon_{\text{domain}} + \sqrt{\frac{5}{8}}l\frac{\mathrm{d}\varepsilon_{\text{domain}}}{\mathrm{d}x} = \left(\frac{gx + \sigma_0}{\sigma_{\text{ref}}}\right)^2, \tag{29}$$

where $\varepsilon_{\text{domain}}$ denotes the strain in the domain (i.e., $x < L$). The solution of (29) satisfying the higher-order boundary condition (24) at the free end is

$$\varepsilon_{\text{domain}} = \varepsilon_{\text{classical}} + \frac{2g\sqrt{\frac{5}{8}}l}{\sigma_{\text{ref}}^2}\left[g(\sqrt{\tfrac{5}{8}}l - x) - \sigma_0 - (g\sqrt{\tfrac{5}{8}}l - \sigma_0)\exp\left(-\frac{x}{\sqrt{\frac{5}{8}}l}\right)\right]. \tag{30}$$

A boundary-layer solution near the fixed end $x = L$ must be added to the above domain solution in order to satisfy the higher-order boundary condition (25), i.e., the strain in the bar can be written as

$$\varepsilon \approx \varepsilon_{\text{domain}}(x) + \left(\frac{l_\varepsilon}{l}\right)^2 \varepsilon_{\text{boundarylayer}}(\xi), \tag{31}$$

where

$$\xi = \frac{L - x}{\left(\frac{l_\varepsilon}{l}\right)^2}$$

is the coordinate within the boundary layer, and $\varepsilon_{\text{boundarylayer}}$ is the boundary-layer solution that rapidly decreases to zero away from the fixed end ($x = L$) and does not disturb the solution in the domain. By letting $\left(\frac{l_\varepsilon}{l}\right)^2 \to 0$ (and therefore $x \to L$ with ξ remaining finite), (26) becomes the following governing equation for $\varepsilon_{\text{boundarylayer}}$,

$$\frac{\sigma^2_{\text{boundary}} + \varepsilon_{\text{domain}}|_{x=L}}{\sigma^2_{\text{boundary}}\left(\dfrac{gL+\sigma_0}{\sigma_{\text{ref}}} - \sigma_{\text{boundary}}\right)} \frac{\mathrm{d}\sigma_{\text{boundary}}}{\mathrm{d}\xi} = \frac{15}{\sqrt{\frac{5}{8}}l}, \tag{32}$$

where σ_{boundary} is $\frac{\sigma}{\sigma_{\text{ref}}}$ near $x = L$ and is related to $\varepsilon_{\text{boundarylayer}}$ via (27) by

$$\sigma_{\text{boundary}}(\xi) = \left[\varepsilon_{\text{domain}}|_{x=L} + \sqrt{\frac{5}{8}}l\left(\left.\frac{\mathrm{d}\varepsilon_{\text{domain}}}{\mathrm{d}x}\right|_{x=L} - \frac{\mathrm{d}\varepsilon_{\text{boundarylayer}}}{\mathrm{d}\xi}\right)\right]^{1/2}. \tag{33}$$

The higher-order boundary condition (25) at the fixed end can be expressed in terms of σ_{boundary} as

$$\sigma_{\text{boundary}}\big|_{\xi=0} = \sqrt{\varepsilon_{\text{domain}}|_{x=L}}. \tag{34}$$

The solution of (33) and (34) is

$$\begin{aligned} &\frac{\varepsilon_{\text{domain}}|_{x=L}}{\left(\dfrac{gL+\sigma_0}{\sigma_{\text{ref}}}\right)^2} \ln\frac{\sigma_{\text{boundary}}}{\sqrt{\varepsilon_{\text{domain}}|_{x=L}}} - \left[1 + \frac{\varepsilon_{\text{domain}}|_{x=L}}{\left(\dfrac{gL+\sigma_0}{\sigma_{\text{ref}}}\right)^2}\right] \ln\left|\frac{\sigma_{\text{boundary}} - \dfrac{gL+\sigma_0}{\sigma_{\text{ref}}}}{\sqrt{\varepsilon_{\text{domain}}|_{x=L}} - \dfrac{gL+\sigma_0}{\sigma_{\text{ref}}}}\right| \\ &- \frac{\sqrt{\varepsilon_{\text{domain}}|_{x=L}}}{\dfrac{gL+\sigma_0}{\sigma_{\text{ref}}}}\left(\frac{\sqrt{\varepsilon_{\text{domain}}|_{x=L}}}{\sigma_{\text{boundary}}} - 1\right) = \frac{15\xi}{\sqrt{\frac{5}{8}}l}. \end{aligned} \tag{35}$$

It can be verified that, as $\xi \to +\infty$ (away from the boundary), $\sigma_{\text{boundary}} \to gL + \sigma_0/\sigma_{\text{ref}}$ and $\mathrm{d}\varepsilon_{\text{boundarylayer}}/\mathrm{d}\xi \to 0$, i.e., the boundary-layer solution indeed decreases rapidly away from the fixed end ($x = L$). The integration of $\mathrm{d}\varepsilon_{\text{boundarylayer}}/\mathrm{d}\xi$ gives $\varepsilon_{\text{boundarylayer}}$, with the integration constant determined from the remote boundary condition, $\varepsilon_{\text{boundarylayer}}(\xi \to +\infty) = 0$.

Figure 2 shows the distribution of $\mathrm{d}\varepsilon/\mathrm{d}x$ in the bar for both MSG and classical plasticity solutions, where $\mathrm{d}\varepsilon/\mathrm{d}x$ is normalized by $g^2L/\sigma^2_{\text{ref}}$; the position x is normalized by the length L of the bar; g and σ_{ref} are the body force and the reference stress in uniaxial tension, respectively. The applied stress at the free end ($x = 0$) takes a value $\sigma_0 = gL$. The length of the bar $L = l$, and the other material length $l_\varepsilon = l/10$, where l is the intrinsic material length in MSG plasticity plasticity. Because L is the same as l, the strain gradient effect is significant over the entire bar such that the curve for MSG plasticity is significantly lower than that for classical plasticity over the entire domain. The curve for MSG plasticity rapidly decreases to zero near the fixed end ($x = L$), displaying the boundary layer effect associated with l_ε.

Figure 3 also shows the distribution of $\mathrm{d}\varepsilon/\mathrm{d}x$ in the bar for the same material parameters, but the bar is much longer, $L = 10l$. Away from both ends ($x = 0$ and $x = L$), the curves for MSG plasticity and classical plasticity are close because $L \gg l$ such that the strain gradient effect is not significant except near the boundaries. The curves for MSG and classical plasticity theories separate apart near the free end ($x = 0$), which reflects the strain gradient effect.

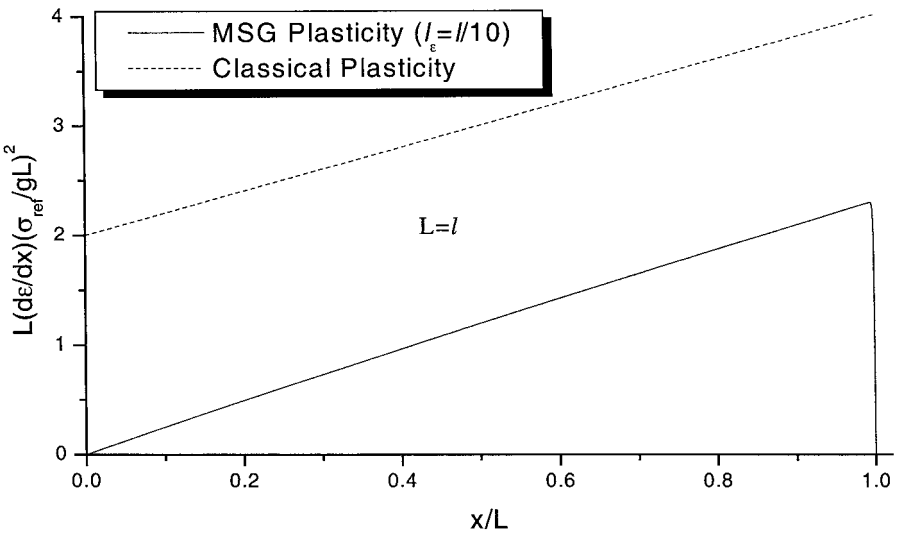

Figure 2. The distribution of strain gradient $\mathrm{d}\varepsilon/\mathrm{d}x$ in the bar for a relatively short bar, $L = l$, where L is the length of the bar, l is the intrinsic material length in strain gradient plasticity; g, σ_0 and σ_{ref} are the body force, applied stress at the free end, and the reference stress in uniaxial tension, respectively, and $\sigma_0 = gL$; the mesoscale cell size $l_\varepsilon = l/10$.

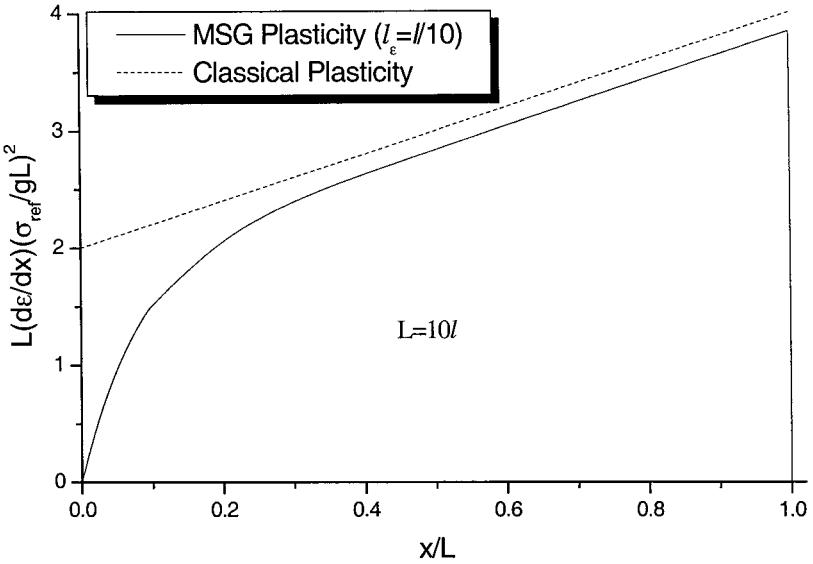

Figure 3. The distribution of strain gradient $\mathrm{d}\varepsilon/\mathrm{d}x$ in the bar for a relatively long bar, $L = 10l$, where L is the length of the bar, l is the intrinsic material length in strain gradient plasticity; g, σ_0 and σ_{ref} are the body force, applied stress at the free end, and the reference stress in uniaxial tension, respectively, and $\sigma_0 = gL$; the mesoscale cell size $l_\varepsilon = l/10$.

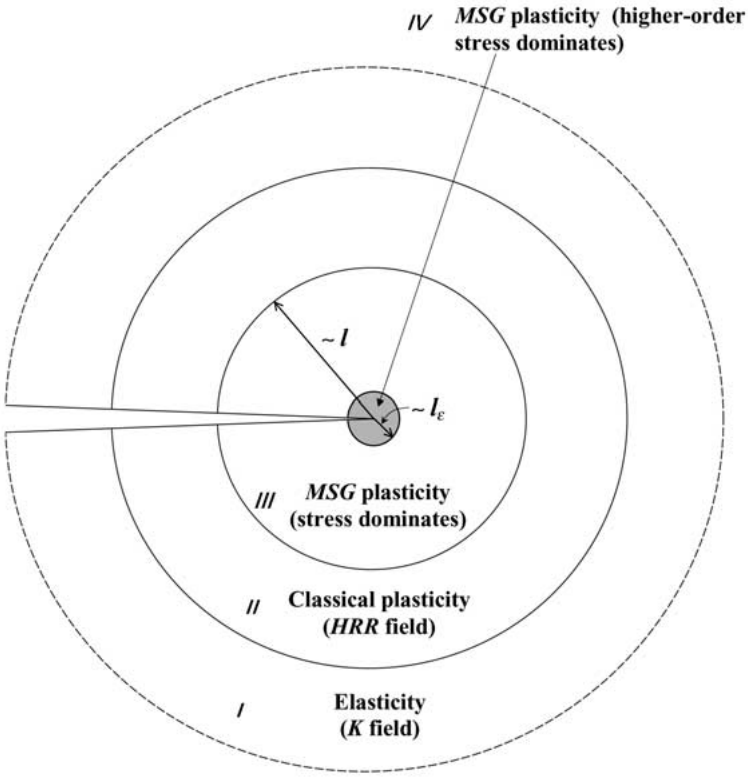

Figure 4. A schematic diagram of different zones surrounding the crack tip, including the elastic K field, HRR field in classical plasticity, the stress-dominated and higher-order stress dominated fields in MSG plasticity.

Around the other end ($x = L$), the boundary layer associated with l_ε is once again clearly observed.

This example demonstrates that there is a boundary layer effect in MSG plasticity associated with the parameter l_ε. Away from the boundary layer, the solution can be obtained by taking $l_\varepsilon = 0$, but this solution is still different from the classical plasticity solution due to the strain gradient effect.

4. Crack tip field in MSG plasticity

Figure 4 is a schematic diagram of different annuli surrounding the crack tip. Far away from the tip, deformation is elastic and the annulus (marked by I in Figure 4) corresponds to the classical elastic K field. The next annulus (*II* in Figure 4) represents the plastic zone inside which the HRR field in classical plasticity dominates. As the distance to crack tip decreases to the order of intrinsic material length l in strain gradient plasticity, the strain gradient effect becomes significant and the third annulus appears (*III* in Figure 4). The finite element analysis (Jiang et al., 2001) showed that the stress level in this zone is two to three times higher than that in the HRR field, and the stress singularity [λ in (1)] is higher than $\frac{1}{2}$, i.e., the stress is more singular than not only the HRR field, but also the classical elastic K field. The higher-order stress is very small as compared to the stress in this zone. Accordingly, the solution in zone *III* is called the stress-dominated MSG plasticity solution (Figure 4). As the distance to the crack

tip decreases further and becomes as small as the mesoscale cell size l_ε in MSG plasticity (which is much smaller than l), the higher-order stress begins to dominate. The solution in this zone, marked by IV in Figure 4, is the so-called higher-order stress dominated MSG plasticity solution. Shi et al. (2000) investigated the asymptotic crack tip field in this zone and established that the higher-order stress dominated asymptotic crack tip field in MSG plasticity is not separable [see (1)].

We focus on the separable asymptotic field inside zone *III* (Figure 4), i.e., at a distance much larger than l_ε such that the higher-order stress is negligible and the stress dominates. Similar to the example in Section 3, the higher-order boundary condition cannot be met on the crack face unless a boundary-layer solution is added to the domain solution given in this section. As shown in the following, the domain solution (i.e., away from the crack face) has a separable field, and the resulting stress singularity is around 0.65, consistent with that reported in the finite element analysis (Jiang et al., 2001). We study the mode *III* crack tip field first since it has a much simpler domain solution than the mode-I counterpart given at the end of this section.

4.1. Mode III crack tip field in MSG plasticity

The out-of-plane displacement in anti-plane deformation is $u_3 = w(x_1, x_2)$, where (x_1, x_2) are the Cartesian coordinates with the origin at the crack tip and the crack faces coinciding with the negative x_1 axis. The annulus *III* in Figure 4 is characterized by

$$l > r \gg l_\varepsilon. \tag{36}$$

A separable displacement w in this annulus can be written as

$$w = r^{2-2\lambda}\,\widetilde{w}(\theta), \tag{37}$$

where (r, θ) are the polar coordinates with $\theta = \pm\pi$ being the crack faces, $\widetilde{w}(\theta)$ is the corresponding angular function of w, and λ, as shown later, is the power of stress singularity to be determined and $\lambda < 1$ as required by the boundedness of the displacement at the crack tip. The corresponding strain field is

$$\varepsilon_{3r} = \varepsilon_{r3} = (1-\lambda)\, r^{1-2\lambda}\widetilde{w}(\theta), \qquad \varepsilon_{3\theta} = \varepsilon_{\theta 3} = \tfrac{1}{2} r^{1-2\lambda}\widetilde{w}'(\theta). \tag{38}$$

The effective strain and effective strain gradient can be obtained as

$$\varepsilon = r^{1-2\lambda}\widetilde{\varepsilon}(\theta) \equiv r^{1-2\lambda}\{\tfrac{4}{3}(1-\lambda)^2\,\widetilde{w}^2 + \tfrac{1}{3}\widetilde{w}'^2\}^{1/2}, \tag{39}$$

$$\begin{aligned}\eta &= r^{-2\lambda}\widetilde{\eta}(\theta)\\ &\equiv r^{-2\lambda}\{(1-\lambda)^2(1-2\lambda)^2\,\widetilde{w}^2 + [\tfrac{1}{2}\widetilde{w}'' + (1-\lambda)\,\widetilde{w}]^2 + \tfrac{1}{2}(1-2\lambda)^2\,\widetilde{w}'^2\}^{1/2}.\end{aligned} \tag{40}$$

For a material point in annulus *III* (Figure 4) with the distance r to the crack tip characterized by (36), the strain gradient becomes significantly larger than the strain such that the flow stress in (8) is dominated by the strain gradient term. Accordingly, the flow stress becomes independent of the uniaxial stress-strain relation $\sigma_{\text{ref}} f(\varepsilon)$ and is given by

$$\sigma = \frac{3\alpha\mu\sqrt{2b}}{r^\lambda}\widetilde{\eta}^{1/2}(\theta), \tag{40}$$

where $\widetilde{\eta}(\theta)$ is defined in (40). It becomes clear now that λ is the stress singularity for this stress-dominated MSG plasticity solution in annulus *III* (Figure 4).

The deviatoric stress can be obtained from the constitutive law (10) while the hydrostatic stress vanishes in anti-plane deformation. The higher-order stress, which scales with l_ε^2, becomes negligible in this stress-dominated solution in annulus *III*. The equilibrium equation (3) gives the following third-order ODE for $\widetilde{w}$ as

$$2(1-\lambda)^2 \frac{\widetilde{w}}{\widetilde{\varepsilon}} \widetilde{\eta}^{\frac{1}{2}} + \frac{\mathrm{d}}{\mathrm{d}\theta}\left\{ \frac{\widetilde{w}'}{\widetilde{\varepsilon}}\, \widetilde{\eta}^{1/2} \right\} = 0. \tag{42}$$

Only the upper half plane ($\theta \geq 0$) is analyzed. The anti-symmetry condition at $\theta = 0$ requires

$$\widetilde{w}\big|_{\theta=0} = 0, \qquad \widetilde{w}''\big|_{\theta=0} = 0. \tag{43}$$

The vanishing of stress traction on the crack face gives

$$\widetilde{w}'\big|_{\theta=\pi} = 0, \tag{44}$$

while the vanishing of higher-order stress traction on the crack face becomes

$$l_\varepsilon^2 \left[2(1-\lambda)\, \widetilde{w}\big|_{\theta=\pi} + \widetilde{w}''\big|_{\theta=\pi} \right] = 0. \tag{45}$$

Only two anti-symmetry conditions at $\theta = 0$ in (43) and the stress traction condition (44) on the crack face can be imposed for the third-order ODE in (42). The resulting domain solution does not satisfy the higher-order stress traction condition (45). Similar to the example in Section 3, a boundary-layer solution needs to be introduced near the crack face in order to meet (45).

Without losing generality, we may impose a normalization condition for the above eigenvalue problem

$$\widetilde{w}'\big|_{\theta=0} = 1. \tag{46}$$

Since (43) and (46) give three boundary conditions at $\theta = 0$, the ODE (42) can be solved by the standard Runge–Kutta numerical method. The only parameter that remains to be determined is the power of stress singularity, λ, which is solved iteratively by the numerical shooting method (Press et al., 1986) in order to meet the stress traction-free condition (44) on the crack face.

The numerical solution gives the power of stress singularity λ_{III} and the stress-dominated asymptotic field around a mode-*III* crack tip in MSG plasticity,

$$\lambda_{III} = 0.65717, \qquad \sigma_{3\alpha} = \sigma_{\alpha 3} = \frac{A_{III}}{r^{\lambda_{III}}}\, \widetilde{\sigma}_{3\alpha}(\theta), \tag{47}$$

where the subscript *III* corresponds to mode *III*, A_{III} is the amplitude factor depending on the loading, specimen geometry and material properties, $\widetilde{\sigma}_{3\alpha}(\theta)$ is the angular distribution, and $\widetilde{\sigma}_{3\theta}\big|_{\theta=0} = 1$. It is observed that the stress field in MSG plasticity $\left(\sim r^{-0.66}\right)$ is indeed more singular than the HRR field and the classical elastic K field $\left(\sim r^{-0.5}\right)$, consistent with the finite element analysis (Jiang et al., 2001).

Figure 5 shows the angular distribution of stress, $\widetilde{\sigma}_{3r}$ and $\widetilde{\sigma}_{3\theta}$, for the stress-dominated crack tip field in MSG plasticity. The mode-*III* elastic K field is also shown for comparison. The angular distributions are normalized such that $\widetilde{\sigma}_{3\theta}\big|_{\theta=0} = 1$. The angular distributions $\widetilde{\sigma}_{3\theta}$

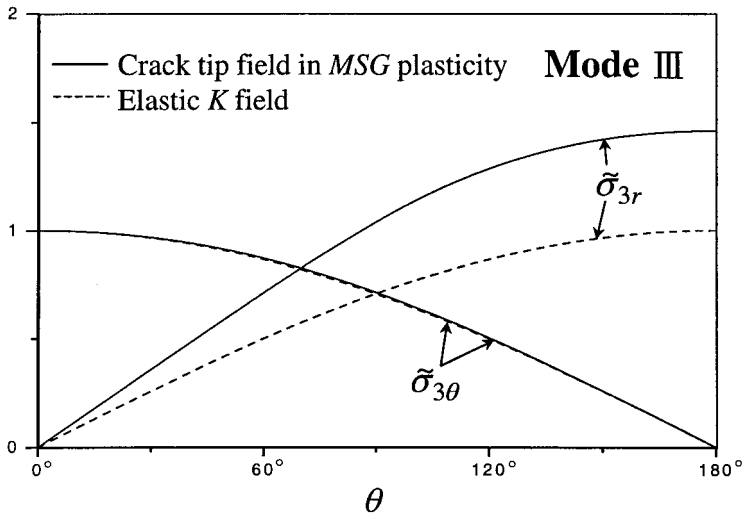

Figure 5. Angular distribution of the stress-dominated asymptotic field around a mode-*III* crack tip in MSG plasticity; $\widetilde{\sigma}_{3\theta}\big|_{\theta=0} = 1$. The mode-*III* elastic K field is also shown.

are almost identical, but the difference in $\widetilde{\sigma}_{3r}$ is significant. However, it should be emphasized that the main difference between the stress-dominated crack tip field in MSG plasticity and the elastic K field in mode *III* is the power of stress singularity.

4.2. Mode I crack tip field in MSG plasticity

Because the deformation is incompressible around a plane-strain mode I crack tip, we may introduce a displacement potential ϕ such that the displacement can be expressed as

$$u_r = -\frac{1}{r}\frac{\partial \phi}{\partial \theta}, \qquad u_\theta = \frac{\partial \phi}{\partial r}. \tag{48}$$

A separable form for ϕ is taken as

$$\phi = r^{3-2\lambda}\,\widetilde{\phi}\,(\theta)\,, \tag{49}$$

where λ is the power of stress singularity to be determined, and $\widetilde{\phi}\,(\theta)$ is the angular distribution of ϕ. The strain and strain gradient fields can be written as

$$\begin{aligned} \varepsilon_{\alpha\beta} &= r^{1-2\lambda}\,\widetilde{\varepsilon}_{\alpha\beta}\,(\theta)\,, & \varepsilon &= r^{1-2\lambda}\,\widetilde{\varepsilon}\,(\theta)\,, \\ \eta_{\alpha\beta\gamma} &= r^{-2\lambda}\,\widetilde{\eta}_{\alpha\beta\gamma}\,(\theta)\,, & \eta &= r^{-2\lambda}\,\widetilde{\eta}\,(\theta)\,, \end{aligned} \tag{50}$$

where the angular functions are determined in terms of $\widetilde{\phi}\,(\theta)$ via the kinematic relations (2) and $\widetilde{\varepsilon}_{\alpha\alpha} = \widetilde{\eta}_{\gamma\alpha\alpha} = 0$ due to incompressibility. The flow stress and deviatoric stress are obtained from the constitutive law (8) and (10), respectively,

$$\sigma = \frac{3\alpha\mu\sqrt{2b}}{r^\lambda}\,\widetilde{\eta}^{1/2}\,(\theta)\,, \qquad \sigma'_{\alpha\beta} = \frac{2\alpha\mu\sqrt{2b}}{r^\lambda}\,\frac{\widetilde{\eta}^{1/2}\,(\theta)}{\widetilde{\varepsilon}\,(\theta)}\,\widetilde{\varepsilon}_{\alpha\beta}\,(\theta)\,. \tag{51}$$

The hydrostatic stress H also takes a separable form

$$H = \frac{2\alpha\mu\sqrt{2b}}{r^\lambda}\,\frac{\widetilde{\eta}^{1/2}\,(\theta)}{\widetilde{\varepsilon}\,(\theta)}\,\widetilde{H}\,(\theta)\,, \tag{52}$$

where the angular function $\widetilde{H}(\theta)$ is to be determined.

Similar to the mode-*III* asymptotic field in Section 4.1, the higher-order stress is negligible in annulus *III* (Figure 4). The equilibrium Equation (3) gives the following two ODEs for angular function $\widetilde{\phi}(\theta)$ and $\widetilde{H}(\theta)$,

$$\begin{aligned} -\frac{\widetilde{\eta}^{1/2}}{\widetilde{\varepsilon}}\left[(2-\lambda)\,\widetilde{\varepsilon}_{\theta\theta}+\lambda\widetilde{H}\right]+\frac{\mathrm{d}}{\mathrm{d}\theta}\left[\frac{\widetilde{\eta}^{1/2}}{\widetilde{\varepsilon}}\,\widetilde{\varepsilon}_{r\theta}\right] &= 0, \\ (2-\lambda)\,\frac{\widetilde{\eta}^{1/2}}{\widetilde{\varepsilon}}\,\widetilde{\varepsilon}_{r\theta}+\frac{\mathrm{d}}{\mathrm{d}\theta}\left[\frac{\widetilde{\eta}^{1/2}}{\widetilde{\varepsilon}}\left(\widetilde{\varepsilon}_{\theta\theta}+\widetilde{H}\right)\right] &= 0. \end{aligned} \tag{53}$$

The symmetry condition at $\theta = 0$ requires

$$\widetilde{\phi}\Big|_{\theta=0} = 0, \qquad \widetilde{\phi}''\Big|_{\theta=0} = 0. \tag{54}$$

By requiring that all angular functions and their derivatives be bounded at $\theta = 0$, the first equation of (53) gives an additional boundary condition at $\theta = 0$,

$$-(2-\lambda)\,\widetilde{\varepsilon}_{\theta\theta}\Big|_{\theta=0} - \lambda\widetilde{H}\Big|_{\theta=0} + \frac{\mathrm{d}\widetilde{\varepsilon}_{r\theta}}{\mathrm{d}\theta}\Big|_{\theta=0} = 0. \tag{55}$$

The vanishing of stress tractions on the crack face gives

$$\left(\widetilde{\varepsilon}_{\theta\theta}+\widetilde{H}\right)\Big|_{\theta=\pi} = 0, \qquad \widetilde{\varepsilon}_{r\theta}\Big|_{\theta=\pi} = 0, \tag{56}$$

while the vanishing of higher-order stress traction on the crack face becomes

$$l_\varepsilon^2\ (\widetilde{\eta}_{\theta\theta r}+\widetilde{\eta}_{r\theta\theta}) = 0. \tag{57}$$

Only three conditions at $\theta = 0$ in (54) and (55) and two stress traction conditions in (56) can be imposed for the fifth ODE in (53). The resulting domain solution does not satisfy the higher-order stress traction condition (57). Similar to the example in Section 3, a boundary-layer solution needs to be introduced on the crack face in order to meet (57).

Without losing generality, we may impose a normalization condition for the above eigenvalue problem

$$\widetilde{\phi}'\big|_{\theta=0} = \sin\beta_0, \quad \widetilde{\phi}'''\big|_{\theta=0} = \cos\beta_0, \quad (0 \le \beta_0 \le \pi)\,. \tag{58}$$

such that $\sqrt{\left(\widetilde{\phi}'\big|_{\theta=0}\right)^2+\left(\widetilde{\phi}'''\big|_{\theta=0}\right)^2} = 1$. For a given power of stress singularity λ and angle β_0, the fifth-order ODE in (53) can be solved by the standard Runge–Kutta numerical method since (54), (55) and (58) give five boundary conditions at $\theta = 0$. The parameters λ and β_0 are then determined iteratively by the shooting method (Press et al., 1986) in order to meet two crack-face stress-traction free conditions in (56).

The numerical solution gives the power of stress singularity λ_I and the stress-dominated asymptotic field around a mode-*I* crack tip in MSG plasticity,

$$\lambda_I = 0.63837, \qquad \sigma_{\alpha\beta} = \frac{A_I}{r^{\lambda_I}}\widetilde{\sigma}_{\alpha\beta}(\theta)\,, \tag{59}$$

where the subscript I corresponds to mode I, A_I and $\widetilde{\sigma}_{\alpha\beta}$ are the amplitude and angular distribution of the mode-I asymptotic field and $\widetilde{\sigma}_{\theta\theta}\big|_{\theta=0} = 1$. The parameter $\beta_0 = 50.071^\circ$. It is observed once again that the stress field in MSG plasticity $\left(r^{-0.64}\right)$ is more singular

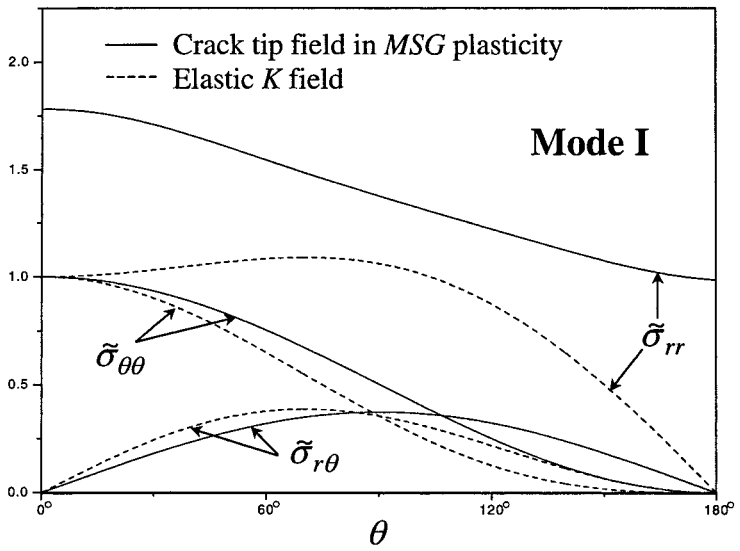

Figure 6. Angular distribution of the stress-dominated asymptotic field around a mode-I crack tip in MSG plasticity; $\widetilde{\sigma}_{\theta\theta}\big|_{\theta=0} = 1$. The mode-$I$ elastic K field (with Poisson's ratio $\nu = 0.5$) is also shown.

than both the HRR field and the classical elastic K field $\left(r^{-0.5}\right)$, consistent with Jiang et al.'s (2001) finite element analysis. In fact, the power of stress singularity λ_I agrees well with that reported in Jiang et al.'s (2001) numerical study. The mode-I stress singularity in MSG plasticity, $\lambda_I = 0.63837$, is slightly smaller than that for mode *III*, $\lambda_{III} = 0.65717$. Even though this has not been observed in classical elastic or elastic-plastic crack tip fields, similar observations have been made in other strain gradient plasticity theories. For example, Huang et al. (1995, 1997) and Xia and Hutchinson (1996) showed that the stress traction ahead of a mode-I crack tip predicted by Fleck and Hutchinson's couple-stress theory of strain gradient plasticity (Fleck and Hutchinson, 1993; Fleck et al., 1994) has the same singularity as the field, while the stress traction ahead of a mode-*III* crack tip has a stronger singularity (Zhang et al., 1998). It should also be pointed out that, unlike the HRR field in classical plasticity, the power of stress singularity in MSG plasticity (λ_I or λ_{III}) is independent of the plastic work hardening exponent N. This is because the strain gradient becomes more singular than the strain near the crack tip and dominates the contribution to the flow stress in (8). This indicates that the density ρ_G of geometrically necessary dislocations around a crack tip is significantly larger than the density ρ_S of statistically stored dislocations.

Figure 6 shows the angular distribution of stress, $\widetilde{\sigma}_{rr}$, $\widetilde{\sigma}_{\theta\theta}$ and $\widetilde{\sigma}_{r\theta}$, for the stress-dominated crack tip field in MSG plasticity and the mode-I elastic K field. The angular distributions are normalized such that $\widetilde{\sigma}_{\theta\theta}\big|_{\theta=0} = 1$. The differences in $\widetilde{\sigma}_{\theta\theta}$ and $\widetilde{\sigma}_{r\theta}$ between the two fields are not significant, but the difference in $\widetilde{\sigma}_{rr}$ is very large. Figure 7 shows the angular distribution of the Von Mises effective stress for the stress-dominated crack tip field in MSG plasticity, the HRR field in classical plasticity (with the plastic work hardening exponent $N = 0.2$), and the classical elastic K field (with Poisson's ratio $\nu = 0.5$). The normalization condition is the same as in Figure 6, i.e., $\widetilde{\sigma}_{\theta\theta}\big|_{\theta=0} = 1$. The curve for MSG plasticity is similar to that for the HRR field, but is quite different from that for the classical elastic K field. However, it should be emphasized once again the main difference between these fields is the order of stress singularity.

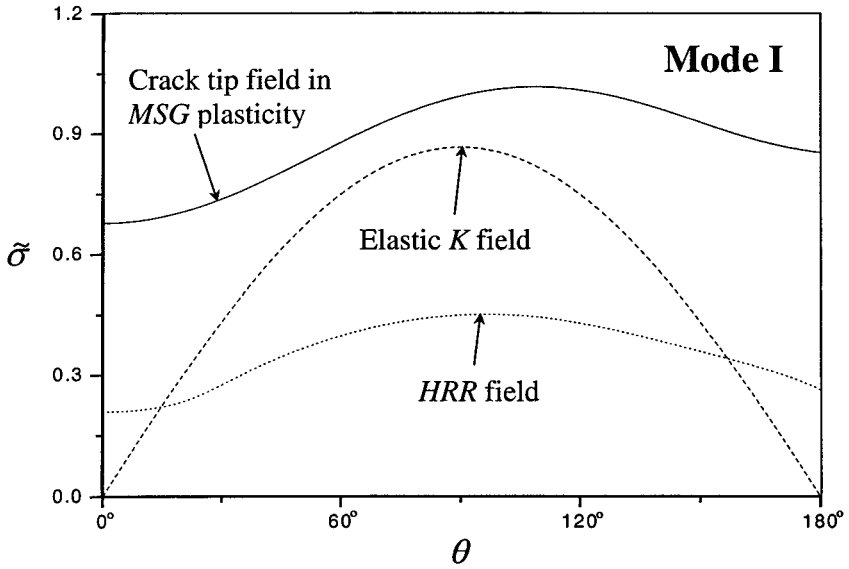

Figure 7. Angular distribution of the effective stress for the stress-dominated asymptotic crack tip field in MSG plasticity, the HRR field in classical plasticity (with plastic work hardening exponent $N = 0.2$), and the mode-I elastic K field (with Poisson's ratio $\nu = 0.5$); $\widetilde{\sigma}_{\theta\theta}\big|_{\theta=0} = 1$.

5. Discussion and conclusions

The separable stress-dominated asymptotic fields around a crack tip in MSG plasticity established in Section 4 are the domain solutions, i.e., they hold in annulus *III* (Figure 4) except near the crack face. Follow the same approach in Section 3, we could add boundary-layer solutions to the domain solutions in Section 4 in order to satisfy the higher-order boundary conditions (45) and (57) on the crack face. But it turns out that the boundary-layer solutions around the crack face are not separable, because the powers r of the separable boundary-layer and domain solutions cannot be matched simultaneously in the equilibrium Equation (3) and higher-order boundary condition (5) on the crack face. This is similar to annulus *IV* (Figure 4) inside which the crack tip field is not separable either (Shi et al., 2000), and one has to solve partial differential equations in order to obtain the non-separable field.

The increase of stress singularity in MSG plasticity (as compared to the HRR field or the classical elastic K field) gives a higher stress level near the crack tip. The finite element analysis of Jiang et al. (2001) indeed showed that, at a distance of approximately 1 μm to the crack tip, the stress level is more than ten times the initial yield stress, which is two to three times higher than the prediction of the HRR field and has reached the stress level to trigger cleavage fracture. This provides an alternative mechanism for cleavage fracture in ductile materials observed in Elssner et al.'s (1994) experiments, i.e., significant stress increase due to geometrically necessary dislocations around the crack tip. For a representative dislocation density $\rho = 10^{16}/\mathrm{m}^2$ of a strain-hardened metal, the average dislocation spacing is on the order of 10 nm. Therefore, the height of the elastic strip surrounding the crack tip in Suo et al.'s (1993) and Beltz et al.'s (1996) dislocation-free zone model is on the order of 10 nm, which is much less than the size l_ε ($\sim$ 100 nm) of the annulus *IV* (Figure 4) immediately surrounding the crack tip. Therefore, we may take a multiscale view for cleavage fracture in ductile materials, i.e., the dislocation-free zone ($\sim$ 10 nm) is surrounded by the crack tip field

in MSG plasticity (annulus *IV* $\sim$ 100 nm, annulus *III* $\sim$ 1 to 10 μm, Figure 4), which in turn is surrounded by the HRR field in classical plasticity (annulus *II*) and the classical elastic K field (annulus *I*) as the distance to the crack tip increases.

In summary, we have demonstrated in the present study that there is a boundary layer effect associated with the mesoscale cell size l_ε in MSG plasticity. The thickness of the boundary layer is on the order of l_ε^2/l ($\sim$ 10 nm), where l is the intrinsic material length in MSG plasticity. By neglecting this boundary layer effect, we have found a stress-dominated asymptotic field around a crack tip in MSG plasticity. The domain of validity for such a field lies in an annulus (*III* in Figure 4) that is approximately between 100 nm to a few microns to the crack tip. The stress in this zone has an approximate singularity of $r^{-2/3}$, and is more singular than not only the HRR field but also the classical elastic K field. The stress level in this zone is significantly ($\sim$ 3 times) higher than the prediction of the HRR field, therefore provides an alternative mechanism for the experimentally observed cleavage fracture in ductile materials.

Acknowledgements

YH acknowledges the support from NSF (grant CMS-0084980 and a supplement to the grant CMS-9896285 from NSF International Program). KCH acknowledges the support from the Ministry of Education, China. The support from NSFC is also acknowledged.

References

Acharya, A. and Bassani, J.L. (2000). Lattice incompatibility and a gradient theory of crystal plasticity. *Journal of Mechanics and Physics of Solids* **48**, 1565–1595.

Acharya A. and Beaudoin A.J. (2000). Grain-size effect in viscoplastic polycrystals at moderate strains. *Journal of Mechanics and Physics of Solids* **48**, 2213-2230.

Aifantis, E.C. (1984). On the microstructural origin of certain inelastic models. *Journal of Engineering Materials and Technology* **106**, 326–330.

Aifantis, E.C. (1992). On the role of gradients in the localization of deformation and fracture. *International Journal of Engineering and Sciences* **30** 1279–1299.

Arsenlis, A. and Parks, D.M. (1999). Crystallographic aspects of geometrically-necessary and statistically-stored dislocation density. *Acta Materials* **47**, 1597–1611.

Ashby, M.F. (1970). The deformation of plastically non-homogeneous alloys. *Philosophical Magazine* **21**, 399–424.

Bagchi, A., Lucas, G.E., Suo, Z. and Evans, A.G. (1994). A new procedure for measuring the decohesion energy of thin ductile films on substrates. *Journal of Materials Research* **9**, 1734–1741.

Bagchi, A. and Evans, A.G. (1996). The mechanics and physics of thin film decohesion and its measurement. *Interface Science* **3**, 169–193.

Begley, M.R. and Hutchinson, J.W. (1998). The mechanics of size-dependent indentation. *Journal of Mechanics and Physics of Solids* **46**, 2049–2068.

Beltz, G.E., Rice, J.R., Shih, C.F. and Xia, L. (1996). A self-consistent model for cleavage in the presence of plastic flow. *Acta Materials* **44**, 3943–3954.

Beltz G.E. and Wang, J.S. (1992). Crack direction effects along copper sapphire interfaces. *Acta Metallurgica et Materialia* **40**, 1675–1683.

Chen, S.H. and Wang, T.C. (2000). A new hardening law for strain gradient plasticity. *Acta Materials* **48**, 3997–4005.

Chen, J.Y., Wei, Y., Huang, Y., Hutchinson, J.W. and Hwang, K.C. (1999). The crack tip fields in strain gradient plasticity: the asymptotic and numerical analyses. *Engeneering Fracture Mechanics* **64**, 625–648.

Cleveringa, H.H.M., VanderGiessen, E. and Needleman, A. (1997). Comparison of discrete dislocation and continuum plasticity predictions for a composite material. *Acta Materials* **45**, 3163–3179.

Cleveringa, H.H.M., VanderGiessen, E. and Needleman, A. (1998). Discrete dislocation simulations and size dependent hardening in single slip. *Journal of Physics* IV, **8**, 83–92.

Cleveringa, H.H.M., VanderGiessen, E. and Needleman, A. (1999a). A discrete dislocation analysis of bending. *Internationals Journal of Plasticity* **15**, 837–868.

Cleveringa, H.H.M., VanderGiessen, E. and Needleman, A. (1999b). A discrete dislocation analysis of residual stresses in a composite material. *Philosophical Magazine* **A79**, 893–920.

Cleveringa, H.H.M., VanderGiessen, E. and Needleman, A. (2000). A discrete dislocation analysis of mode I crack growth. *Journal of Mechanics and Physics of Solids*, **48**, 1133–1157.

Cottrell, A.H. (1964). *The Mechanical Properties of Materials*, J. Willey, New York, 277.

Dai, H. and Parks, D.M. (2001). Geometrically-necessary dislocation density in continuum crystal plasticity theory and FEM implementation (unpublished manuscript).

de Borst R. and Mühlhaus H.-B. (1991). Computational strategies for gradient continuum models with a view to localization of deformation. In *Proceedings of International Conference on Nonlinear Engineering Computation.* (Edited by N. Bićanić, P. Marović, D.R.J. Owen, V. Jović and A. Mihanović), Prineridge Press, Swansea, 239–260.

de Borst R. and Mühlhaus H.-B. (1992). Gradient-dependent plasticity: formulation and algorithmic aspects. *International Journal for Numerical Methods in Engineering* **35**, 521–539.

de Guzman, M.S., Neubauer, G., Flinn, P. and Nix, W.D. (1993). The role of indentation depth on the measured hardness of materials. *Materials Research Symposium Proceedings* **308**, 613–618.

Elssner, G., Korn, D. and Ruehle, M. (1994). The influence of interface impurities on fracture energy of UHV diffusion bonded metal-ceramic bicrystals. *Scripta Metallurgica et Materialia* **31**, 1037–1042.

Fleck, N.A. and Hutchinson, J.W. (1993). A phenomenological theory for strain gradient effects in plasticity. *Journa of Mechanics and Physics of Solids* **41**, 1825–1857.

Fleck, N.A. and Hutchinson, J.W. (1997). Strain gradient plasticity. *Advances in Applied Mechanics* (Edited by J.W. Hutchinson, and T.Y. Wu), Vol 33, Academic Press, New York, 295–361.

Fleck, N.A., Muller, G.M., Ashby, M.F. and Hutchinson, J.W. (1994). Strain gradient plasticity: theory and experiments. *Acta Metallurgica et Materialia* **42**, 475–487.

Gao, H., Huang, Y. and Nix, W.D. (1999a). Modeling plasticity at the micrometer scale. *Naturwissenschaften* **86**, 507–515.

Gao, H., Huang, Y., Nix, W.D. and Hutchinson, J.W. (1999b). Mechanism-based strain gradient plasticity - I. Theory. *Journal of Mechanics and Physics of Solids* **47**, 1239–1263.

Gurtin, M.E. (2000). On the plasticity of single crystals: free energy, microforces, plastic-strain gradients. *Journal of Mechanics and Physics of Solids* **48**, 989–1036.

Huang, Y., Gao, H., Nix, W.D. and Hutchinson, J.W. (2000a). Mechanism-based strain gradient plasticity-II. Analysis. *Journal of Mechanics and Physics of Solids* **48**, 99–128.

Huang, Y., Xue, Z., Gao, H. and Xia, Z.C. (2000b). A study of micro-indentation hardness tests by mechanism-based strain gradient plasticity. *Journal of Materials Research* **15**, 1786–1796.

Huang, Y., Zhang, L., Guo, T.F. and Hwang, K.C. (1995). Near-tip fields for cracks in materials with strain-gradient effects. *Proceedings of IUTAM Symposium on Nonlinear Analysis of Fracture* (Edited by J.R. Willis), Kluwer Academic Publishers, Cambridge, England, 231–242.

Huang, Y., Zhang, L., Guo, T.F. and Hwang, K.C. (1997). Mixed mode near-tip fields for cracks in materials with strain-gradient effects. *Journal of Mechancis and Physics of Solids* **45**, 439–465.

Hutchinson, J.W. (1968). Singular behavior at the end of a tensile crack in a hardening material. *Journal of Mechanics and Physics of Solids* **16**, 13–31.

Hutchinson, J.W. (1997). Linking scales in mechanics. *Advances in Fracture Research* (Edited by B.L. Karihaloo, Y.W. Mai, M.I. Ripley and R.O. Ritchie), Pergamon Press, Amsterdam, 1–14.

Jiang, H., Huang, Y., Zhuang, Z. and Hwang, K.C. (2001). Fracture in mechanism-based strain gradient plasticity. *Journal of Mechanics and Physics of Solids* **49**, 979–993.

Korn D., Elssner, G., Fischmeister, H.F., et al. (1992). Influence of interface impurities on the fracture energy of UHV bonded niobium sapphire bicrystals. *Acta Metallurgica et Materialia* **40**, S355-S360 Suppl. S.

Lasry D. and Belytschko, T. (1988). Localization limiters in transient problems. *International Journal of Solids and Structures* **24**, 581–597.

Ma, Q. and Clarke, D.R. (1995). Size dependent hardness of silver single crystals. *Journal of Materials Research* **10**, 853–863.

McElhaney, K.W., Vlassak, J.J. and Nix, W.D. (1998). Determination of indenter tip geometry and indentation contact area for depth-sensing indentation experiments. *Journal of Materials Research* **13**, 1300–1306.

Mühlhaus H.B. and Aifantis E.C. (1991). A variational principle for gradient plasticity. *Interntional Journal of Solids and Structures* **28**, 845–857.

Needleman, A. (2000). Computational mechanics at the mesoscale. *Acta Materialia* **48**, 105–124.

Nix, W.D. (1989). Mechanical properties of thin films. *Materials Transactions A* **20A**, 2217–2245.

Nix, W.D. (1997). Elastic and plastic properties of thin films on substrates: nanoindentation techniques. *Materials Science and Engineering A-Struct.* **234**, 37–44.

Nix, W.D. and Gao, H. (1998). Indentation size effects in crystalline materials: a law for strain gradient plasticity. *Journal of Mechanics and Physics of Solids* **46**, 411–425.

Nye, J.F. (1953). Some geometrical relations in dislocated crystals. *Acta Metallurgica et Materialia* **1**, 153–162.

O'Dowd, N.P., Stout, M.G. and Shih, C.F. (1992). Fracture-toughness of alumina niobium interfaces - experiments and analyses. *Philosophical Magazine A* **66**, 1037–1064.

Oh, T.S., Cannon, R.M. and Ritchie, R.O. (1987). Subcritical crack growth along ceramic-metal interfaces. *Jom-Journal of Minerals, Metals and Materials S* **39**, A57–A57.

Poole, W.J., Ashby, M.F. and Fleck, N.A. (1996). Micro-hardness of annealed and work-hardened copper polycrystals. *Scripta Matererialia* **34**, 559–564.

Press, W.H., Flannery, B.P. Teukolsky, S.A. and Vetterling, W.T. (1986). *Numerical Recipes*, Cambridge University Press, Cambridge.

Rice, J.R. and Rosengren, G.F. (1968). Plane strain deformation near a crack tip in a power law hardening material. *Journal of Mechanics and Physics of Solids* **16**, 1–12.

Shi, M., Huang, Y., Gao, H. and Hwang, K.C. (2000). Non-existence of separable crack tip field in mechanism-based strain gradient plasticity. *International Journal of Solids and Structures* **37**, 5995–6010.

Shu, J.Y. and Fleck, N.A. (1999). Strain gradient crystal plasticity: size-dependent deformation of bicrystals. *Journal of Mechanics and Physics of Solids* **47**, 297–324.

Sluys L.J., de Borst, R. and Mühlhaus H.B. (1993). Wave-propagation, localization and dispersion in a gradient-dependent medium. *International Journal of Solids and Structures* **30**, 1153–1171.

Stelmashenko, N.A., Walls, A.G., Brown, L.M. and Milman, Y.V. (1993). Microindentation on W and Mo oriented single crystals: an STM study. *Acta Metallurgica et Materialia* **41**, 2855–2865.

Stolken, J.S. and Evans, A.G. (1998). A microbend test method for measuring the plasticity length scale. *Acta Materialia* **46**, 5109–5115.

Suo, Z., Shih, C.F. and Varias A.G. (1993). A theory for cleavage cracking in the presence of plastic-flow. *Acta Metallurgica et Materialia* **41** 1551–1557.

Suresh S., Nieh, T.G. and Choi, B.W. (1999). Nano-indentation of copper thin films on silicon substrates. *Scripta Materialia* **41**, 951–957.

Taylor, G.I. (1938). Plastic strain in metals. *Journal of the Institute of Metals* **62**, 307–324.

Wang, J.-S. and Anderson, P.M. (1991). Fracture behavior of embrittled FCC metal bicrystals and its misorientation dependence. *Acta Metallurgica et Materialia* **39**, 779–792.

Wei, Y. and Hutchinson, J.W. (1997). Steady-state crack growth and work of fracture for solids characterized by strain gradient plasticity. *Journal of Mechanics and Physics of Solids* **45**, 1253–1273.

Wei, Y. and Hutchinson, J.W. (1999). Models of interface separation accompanied by plastic dissipation at multiple scales. *International Journal of Fracture* **95**, 1–17.

Zbib H.M. and Aifantis E.C. (1988). On the localization and postlocalization behavior of plastic deformation. Part I. On the initiation of shear bands; Part II. On the evolution and thickness of shear bands. Part III. On the structure and velocity of Portevin-Le Chatelier bands. *Res. Mech.*, 261–277, 279–292 and 293–305.

Zhang L., Huang Y., Chen J.Y. and Hwang K.C. (1998). The mode III full-field solution in elastic materials with strain gradient effects. *International Journal of Fracture* **92**, 325–348.